Integrated stratigraphy of the Maikop type section (Republic of Adygea, Russia)

MSc thesis Kevin Vis, April 2018
Department of Earth Sciences – Utrecht University

Abstract

The commercially relevant Maikop group lacks abundant microfossils and ash layers, which makes dating of the sediments problematic. This thesis project aims to construct an age frame for this sedimentary sequence deposited in the former Paratethys region. Using new paleomagnetic data from the Maikop group type section at the Belaya River, together with existing biostratigraphic data, a first attempt is made at dating the entirety of the early Oligocene to Middle Miocene Maikop group. Two possible correlations are presented. One based on previous and ongoing paleomagnetic research on parts of the Maikop group and the other on expected stable sedimentation and biostratigraphic zones. A detailed investigation on the base of the Maikop group and upper Belaya Glina formation shows the lower boundary of the Maikop group coincides with the C13r-C13n reversal, resulting in an age for the base of the Maikop of 33.71 Ma. This agrees with the hypothesis that the change in sedimentation from light coloured marls to dark organic rich clays at this boundary was the result of a large sea level drop during the Oi-1 event, leading to stratification of the water column which restricted oxygenation of the bottom waters.

1. Introduction

The Maikop group is viewed as one of the most important source rocks for oil and gas in the former Paratethys region (Figure 1) and is also an important source of manganese ore deposits (Hudson et al., 2008; Sachsenhofer and Schulz, 2006; Varentsov et al., 2003). The commercial relevance of Maikop deposits led to an extensive amount of research into the group (Ershov et al., 2003, 1999; Sachsenhofer et al., 2017). Dating of the Maikop group rocks, however, has been difficult due to a lack of microfossils and ash layers (Van der Boon, 2017). Language barriers, political boundaries and highly variable naming conventions in the former Paratethys region make it difficult to correlate the few available data sets that can be used for dating. A recent paleomagnetic study by (Van der Boon, 2017) showed that construction of a magnetostratigraphy for the Kuma and Belaya Glina formations underlying the Maikop group is difficult due to low intensities, but that the construction of a magnetostratigraphy of the lower part of the Maikop group was possible. Van der Boon (2017) located the top of chron C13n based on paleomagnetic and biostratigraphic data and a single ash layer, but could not constrain the bottom of this chron. Van der Boon (2017) found several other changes in polarity higher in the stratigraphy, which are still poorly constrained. Palcu et al. (2018) constructed a magnetostratigraphy for the Tarkhanian, Chokrakian, Karaganian and Konkian formations overlying the Maikop group, which dates the top of the Maikop group at approximately 14.86 Ma. Creation of a magnetostratigraphy for the entire Maikop type-locality section (Republic of Adygea, Russia, figure 2) could solve the troublesome dating of this sedimentary succession and will make correlation with data sets from other sections in the former Paratethys region more viable. This study presents magnetostratigraphy of this section in combination with new and published (Akhmetiev et al., 1995; Gavrilov et al., 2017; Sachsenhofer et al., 2017) biostratigraphic data to construct an integrated stratigraphy for the Maikop type-locality section, with a focus on the boundary between the organic rich Maikop group (Early Oligocene) and the light coloured marls of the underlying Belaya Glina formation (Late Eocene/Early Oligocene), constraining the age of the lower boundary of the Maikop group. Dating of this boundary could help distinguish what exactly caused this change in sediment composition.

1.1 Geologic background

The Maikop group sediments are described as organic rich clays that were deposited in the Paratethys (Sachsenhofer et al., 2017 and references therein), a semi-isolated epicontinental sea (Figure 1). Deposition of these sediments started around the Eocene-Oligocene transition and continued up into the Miocene. The transition to these dark organic rich sediments from the white marls of the underlying Belaya Glina formation (Late Eocene) has been suggested to be caused by (partial) isolation of the Paratethys from the global oceans (Sachsenhofer et al., 2017). This isolation is thought to be caused by a rapid sea level drop (Sachsenhofer et al., 2017) and/or ongoing tectonic activity related to the Arabia-Eurasia collision that started during the Eocene (Allen and Armstrong, 2008). While (Sachsenhofer et al., 2017) suggest this sea level drop within the Paratethys region (Popov et al., 2010) already occurred during Priabonian time, (Van der Boon, 2017) suggests it occurred during the early Oligocene, since the bottom of the Maikop falls within chron C13n, and relates it to the global sea level drop during the Oi-1 event (Houben et al., 2012). Isolation of the Paratethys caused stratification of the water column which restricted oxygenation of bottom waters. Continuous sinking of decomposing organic matter resulted in deoxygenation of these bottom waters, which led to mostly anoxic conditions within the Paratethys (Schulz et al., 2005).

1.2 Maikop type-locality section

The studied section along the Belaya River north of the Greater Caucasus (Republic of Adygea, Russia, figure 2) contains a 635 m thick record of the Maikop group. Except for two erosional levels bounding the Polbian bed all outcropped parts of the section show conformable strata. The Maikop group is subdivided in several formations based on lithology (Figure 4). The definition of these subdivisions and their naming conventions differ per study, depending on time of writing and writer. For the sake of clarity this study uses the formation names used within

the most recent overview (Sachsenhofer et al., 2017) and formation descriptions based on references therein. The Maikop group overlies the light coloured, bioturbated marls of the Belaya Glina formation, which become darker towards the boundary with the Maikop group. The boundary itself is identified as the first significantly darker, several millimetres thick lamina at the base of the laminated dark calcareous shales that make up the Pshekha formation. The contact is conformable in this section. The Psheckha formation contains benthic molluscs, planktonic pteropods and fish remains. The overlying Polbian bed, comprised of a sandy, bioturbated layer and a shaly limestone (± 30 cm), is bounded by two erosional contacts. Going up the section, the Lower Morozkina Balka (LMB) formation consists of laminated non-calcareous clays, while the Upper Morozkina Balka (UMB) formation has high carbonate content. The Batalpashinsk and Septarian formations consist of non-calcareous shales with fish remains. The Septarian formation contains septarian concretions, marl concretions and sandy layers. The overlying silty clays of the Karadzhalga formation contain abundant fish remains. The top Olginskaya and Ritsa formations consist of non-calcareous clays. The Olginskaya formation is bioturbated, while the Ritsa formation is laminated. The orientation of beds in this section is fairly consistent, with dip angles varying between 3 and 20 degrees and dip directions between 350 and 66 degrees (Figure 3). About 60 percent of the Maikop group is exposed in this section (Figure 4).

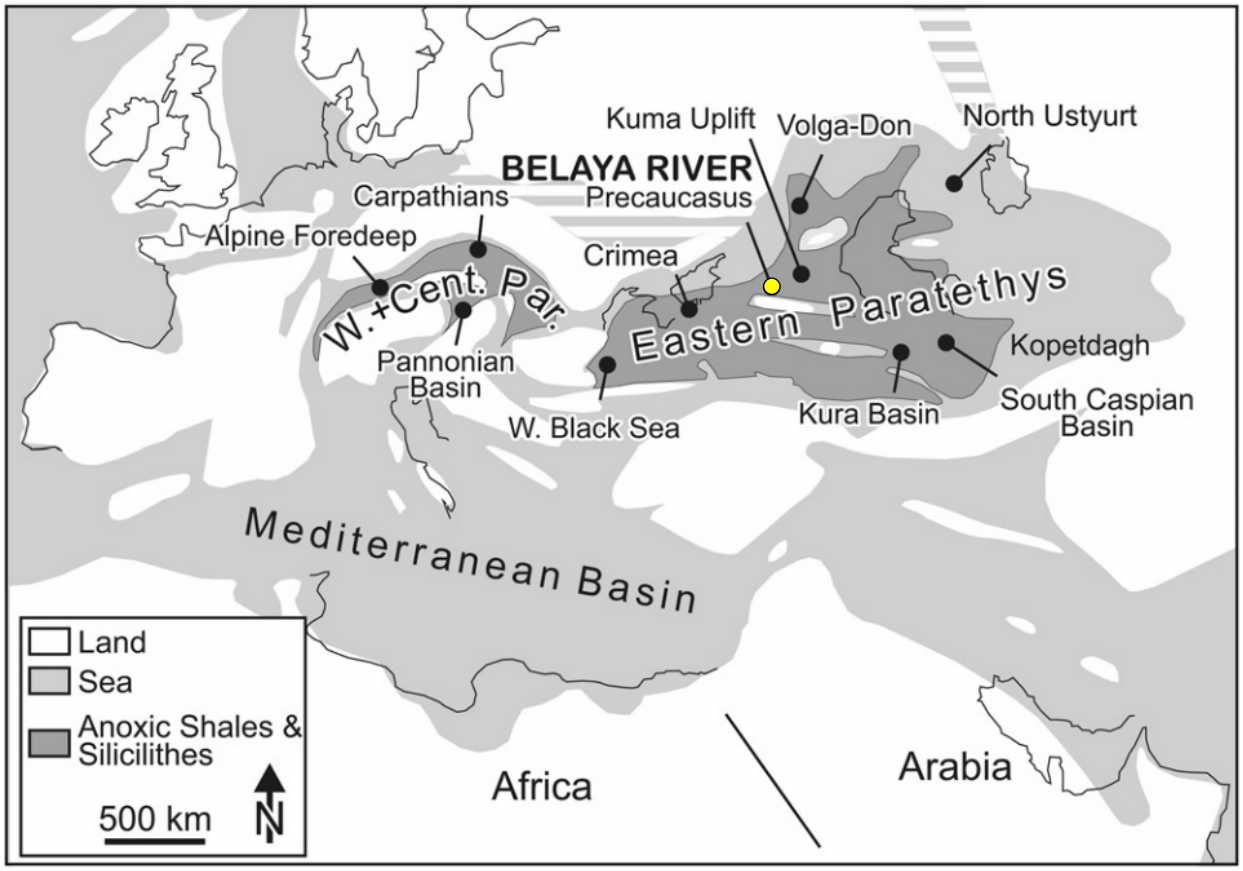

Figure 1. From (Sachsenhofer et al., 2017): Paleogeographic map of the Paratethys during the early Oligocene, simplified after (Popov et al., 2004).

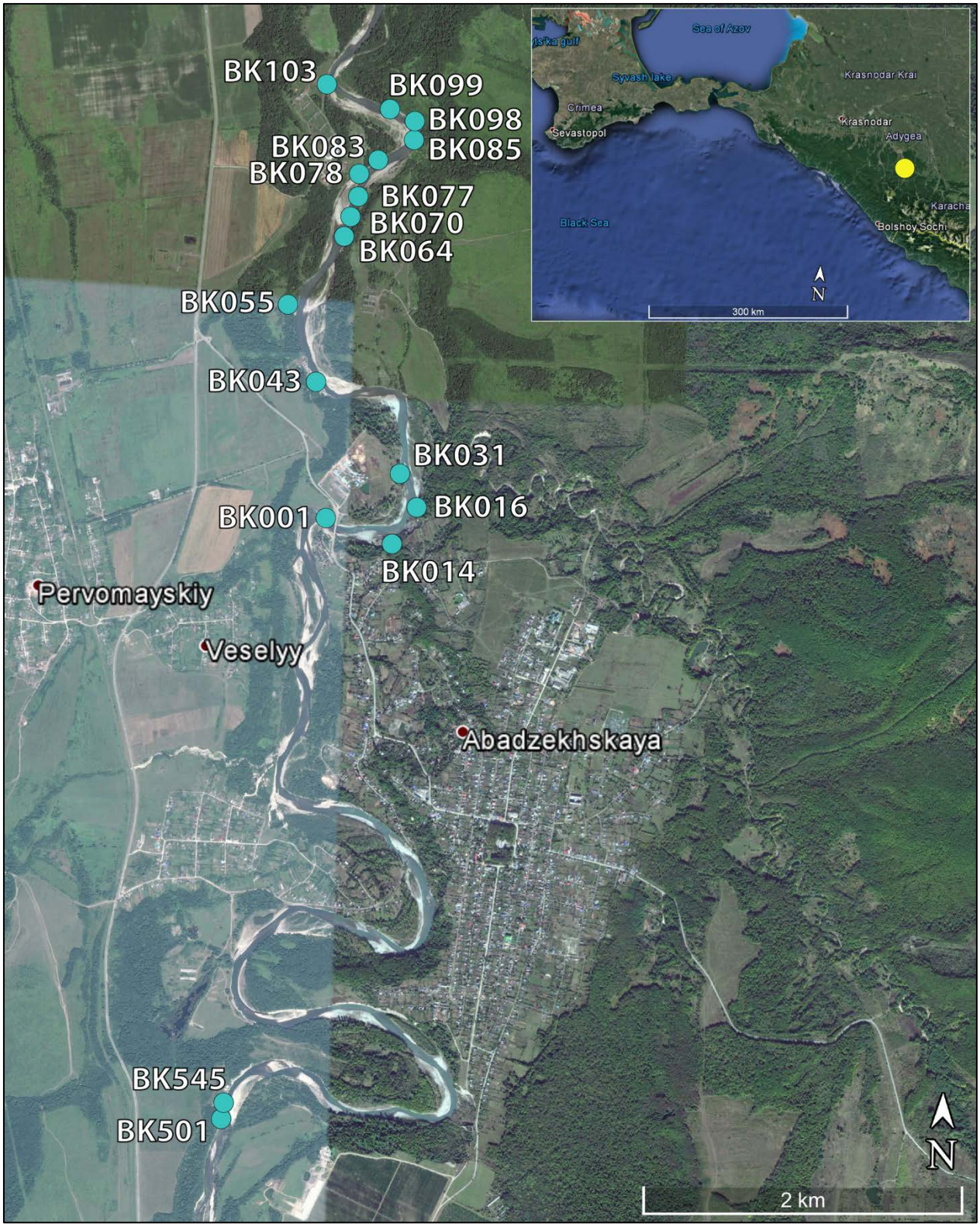

Figure 2. Google Earth image of the sample locations (light blue). The inset shows the location of the study area (yellow dot) in the northern Greater Caucasus (Republic of Adygea, Russia).

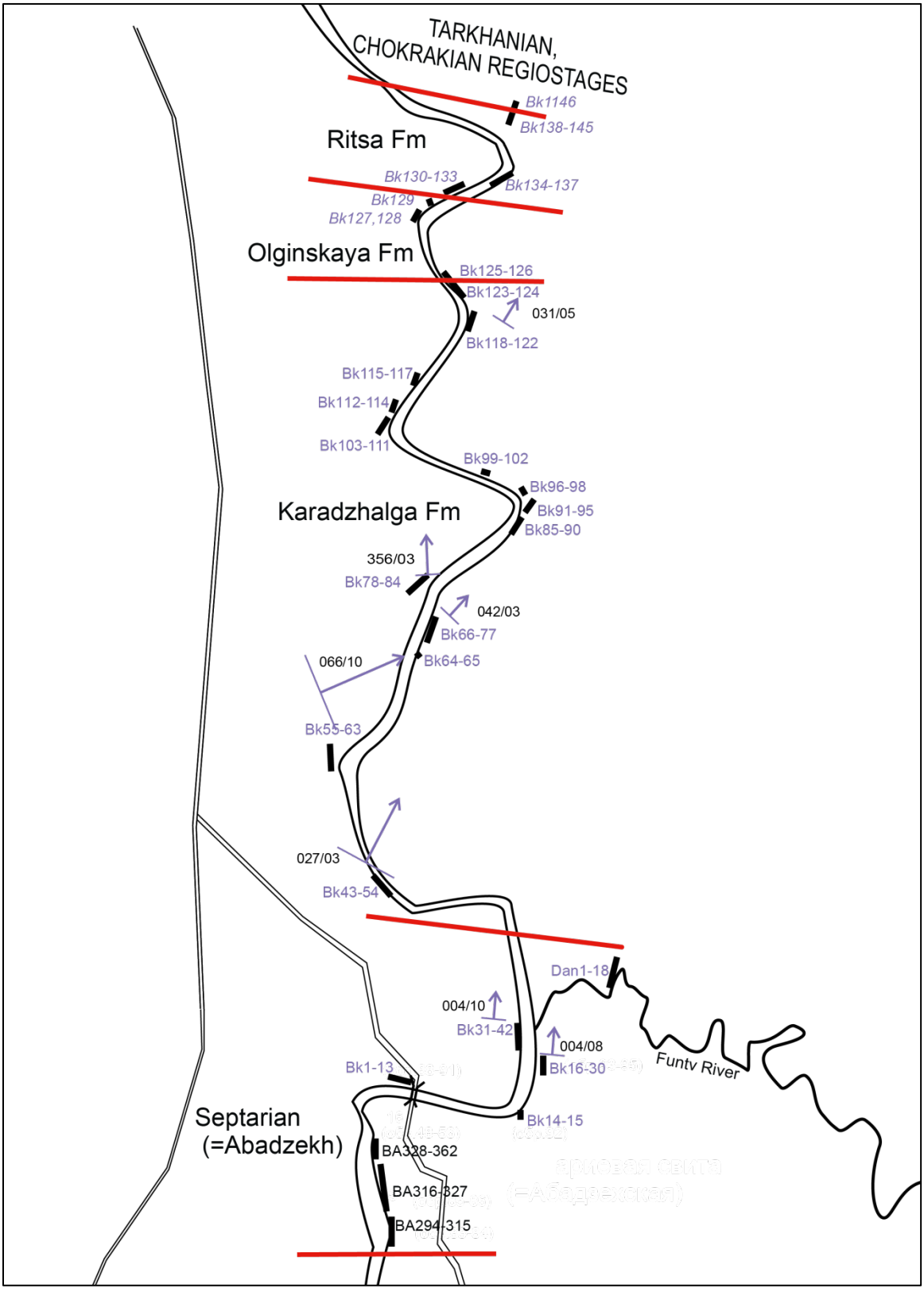

Figure 3. Map of sample locations in the upper formations of the Maikop group with formation boundaries in red and layer orientations in purple with dip direction/dip data. BK samples were taken for this study. BA samples were taken in 2016. Figure modified after figure by S. V. Popov.

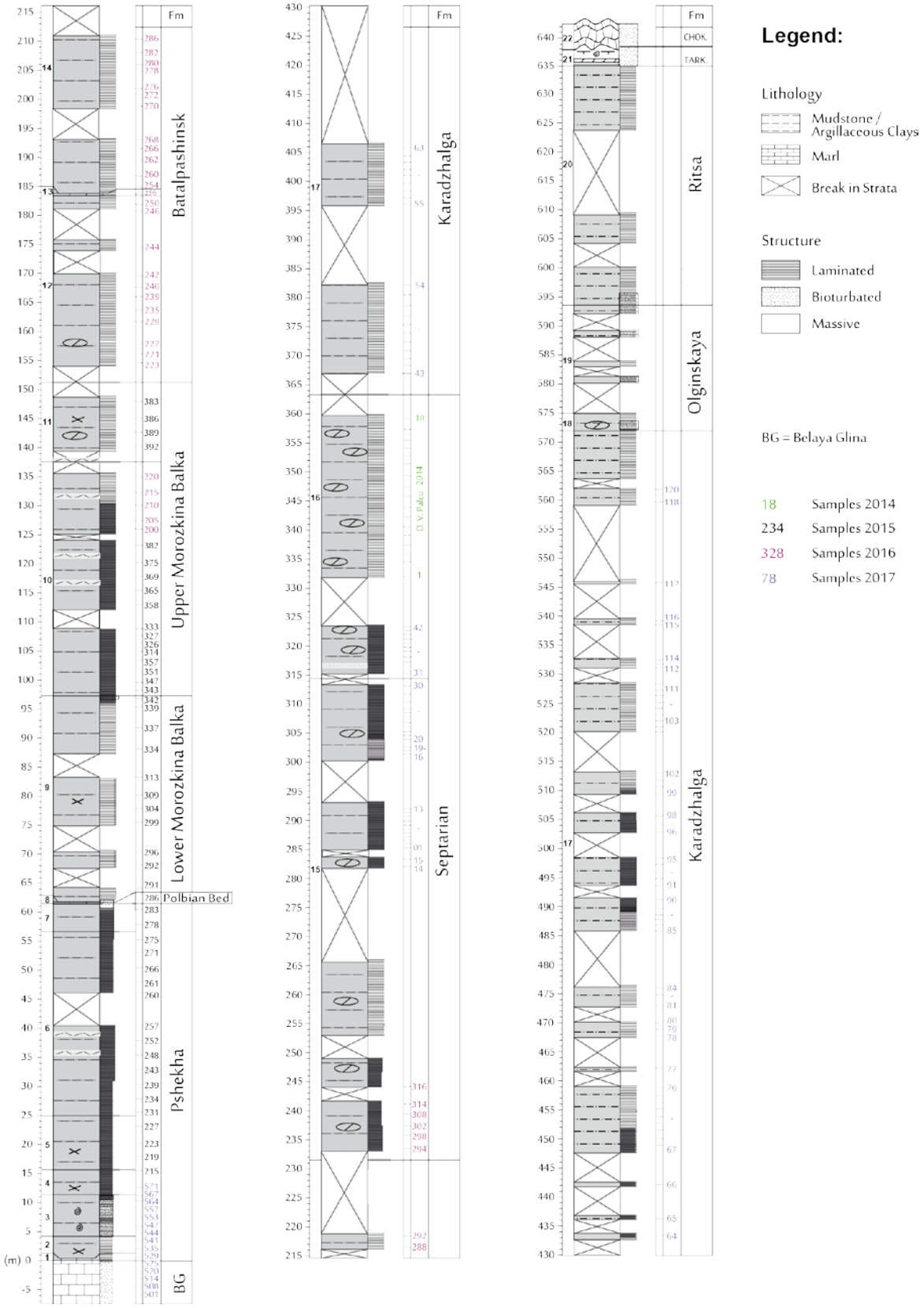

Figure 4. Log of the Maikop Group sediments at the Belaya River modified after figure by S. V. Popov. Shows sample levels from 2014 by D.V. Palcu, from 2015 coded BE, from 2016 coded BA and the sample levels from 2017 taken as part of this study are coded BK.

2. Methods

All paleomagnetic data was acquired at Fort Hoofddijk, paleomagnetic laboratory of Utrecht University. Conventional paleomagnetic samples (25 mm diameter cores) were taken using a gasoline-powered drill and oriented using a magnetic compass. The cores were cut in the laboratory into standard (22 mm) specimens. Core and bedding orientations were corrected for a present day magnetic declination of 7.2° (IGRF). Figure 2 shows sample locations. Samples BK501-BK571 were drilled at 25 cm intervals, starting 5.45 meters below the Belaya Glina-Maikop boundary. About every 5 m the bedding orientation was measured in this part of the section. On each level two samples were drilled, one for thermal demagnetization and one for alternating field demagnetization. Combined with sample sets from field campaigns in 2014 (samples 1-18 by D.V. Palcu in figure 4), 2015 (Van der Boon, 2017) and 2016 (BA200-BA318, processed as part of this study) samples BK001-BK120 (2017; figures 2, 3 & 4) complete a sampling of the entire Maikop group. These samples were taken at 50 to 100 cm intervals. The log in figure 4 shows all sample levels.

2.1 2G Enterprises DC SQUID cryogenic magnetometer

A cryogenic magnetometer (noise level $3*10^{-12}$ $Am^{2)}$ was used to measure the natural remanent magnetization (NRM) of the specimens. Stepwise thermal demagnetisation was performed using a magnetically shielded oven with a residual field less than 10nT. Low expected intensities required all specimens to be measured in 2 positions and results were based on an average of 3 SQUID readings. Heating steps were based on previous research done on the lower part of the Belaya River section done by A. van der Boon and were: 20 – 40 – 60 – 80 – 100 – 115 – 130 – 150 – 170 – 190 – 210 – 230 (- 260 – 280 – 300 – 320 – 340)°C for specimens BK001A-BK066A, and: 20 – 40 – 60 – 80 – 100 – 120 – 140 – 160 – 180 – 200 – 220 – 240 (- 260 – 280 – 300 – 320 – 340)°C for specimens BK067A-BK120A and BA specimens (The temperatures between brackets are extra temperature steps taken with specimens that were not empty after heating up to 230/240 °C.)

2.2 Robotized 2G Enterprises horizontal DC-SQUID magnetometer with in-line AF demagnetization

A total of 144 specimens was measured using a robotized 2G DC-SQUID magnetometer (dynamic range $3*10^{-12}$ to $5*10^{-5}$ Am^2) (Mullender et al., 2016) for alternating field (AF) demagnetization. The first batch of 96 specimens was demagnetized and measured using a 'per component' protocol to prevent gyroremanent magnetization (GRM), because of the suspected presence of greigite in the specimens. After analysis of the results of these measurements however the specimens were generally already empty when the influence of GRM normally starts to alter the results (for fields > 35 mT) and thus the use of this protocol was not deemed necessary for further measurements. The demagnetization steps used were also based on prior measurements done by A. van der Boon and were: 0 – 4 – 8 – 12 – 14 – 16 – 18 – 20 – 22 – 25 – 30 – 35 – 40 – 60 – 80 – 100 mT

2.3 Data processing

Principal component analysis (Kirschvink, 1980) was performed on Zijderveld diagrams (Zijderveld, 1967) using the interpretation portal of palemagnetism.org (Koymans et al., 2016) to calculate declination and inclination angles for pre-tilt (TC) signals. For specimens with multiple components, due to overlapping blocking temperatures or coercivity, planes (great circles) were determined. Both lines and planes in the Zijderveld diagrams presented were constructed using an eigenvector approach (Kirschvink, 1980). When specimens showed unterminated great circle paths, great circle solutions were determined using the method of (McFadden and McElhinny, 1988). Mean inclinations calculated using Fisher statistics (Fischer, 1953) were compared to expected inclination values (GAPWaP, Torsvik et al., 2012; Van Hinsbergen et al., 2015) for the specimens studied.

2.4 Dinoflagellate cyst analysis

Eight samples from around the Belaya Glina-Pshekha boundary were processed for additional palynological analysis by Arjen Grothe. The standard palynological techniques of the Laboratory for Palaeobotany and Palynology, Utrecht University, were used for sample processing (e.g. Brinkhuis et al., 2003). 5-20 grams of material was oven-dried at 60 °C, crushed and weighed. A tablet with a known amount of *Lycopodium clavatum* spores was added to make semi-quantitative estimates. The samples were consequently treated with 30% HCl to remove carbonates and with 38% HF to remove silicates. 250 and 15 µm sieves were used to sieve the remaining solution, after which the remaining fraction was mounted on a slide using glycerine jelly. A light microscope at magnification 400x was used for palynological analysis.

3. Results

3.1 BK500 series

Representative Zijderveld diagrams, equal area projections and intensity plots of the upper part of the Belaya Glina formation (up to and including specimen BK526A) are shown in figure 5 and those of the lower part of the Pshekha formation (from specimen BK527A) are shown in figure 6. Part of the specimens underneath the boundary show a high temperature (220-320 °C) reversed signal (e.g. Figure 5a) or an unterminated great circle path (e.g. Figure 5e, h, k) that indicates a reversed characteristic remanent magnetization (ChRM). All specimens seem to have a large normal overprint (interpreted in specimens BK508A, BK520A and BK526A, figure 5d, g, j) that is partly removed during heating for some of the specimens (e.g. Figure 5g), but is very dominant in other specimens (e.g. Figure 5j). The unterminated great circle path in figure 5k suggests movement of the direction of magnetization towards a reverse ChRM, but this specimen could also be interpreted as showing a normal ChRM. From the Belaya Glina-Pshekha boundary up in the stratigraphy (Specimens BK527A-BK571A) this behaviour is not seen anymore; all specimens show a normal orientation that decreases in intensity along a straight line towards the origin in the Zijderveld diagrams. These specimens do not show movement of the direction of magnetization along a great circle (Figure 6).

The intensity plots in figure 5 show that the Belaya Glina specimens have a very low intensity starting between 100-150 µA/m at room temperature, rapidly decreasing towards around 20 µA/m between 160-200 °C. The only exception is specimen BK520A with a higher starting intensity of 256 µA/m ending at an intensity of 36 µA/m at 340 °C. Within the Pshekha formation (Figure 6) initial intensity is generally higher and more variable, ranging from 130 µA/m to 3620 µA/m. Intensities in this part of the section drop rapidly, to lower than 10% of their initial intensity, during heating up to 160-200 °C. Maximum intensity values for each specimen are plotted in figure 8.

Figure 5 (next page). Representative Zijderveld diagrams (TC), equal area projections with great circles which show the movement of directions of magnetization towards their reversed high temperature component and intensity diagrams showing demagnetization behaviour for specimens BK501A up to BK526A from the Belaya Glina formation. In (a) the high temperature reversed component is plotted. In (d, g & j) the low temperature normal components are plotted.

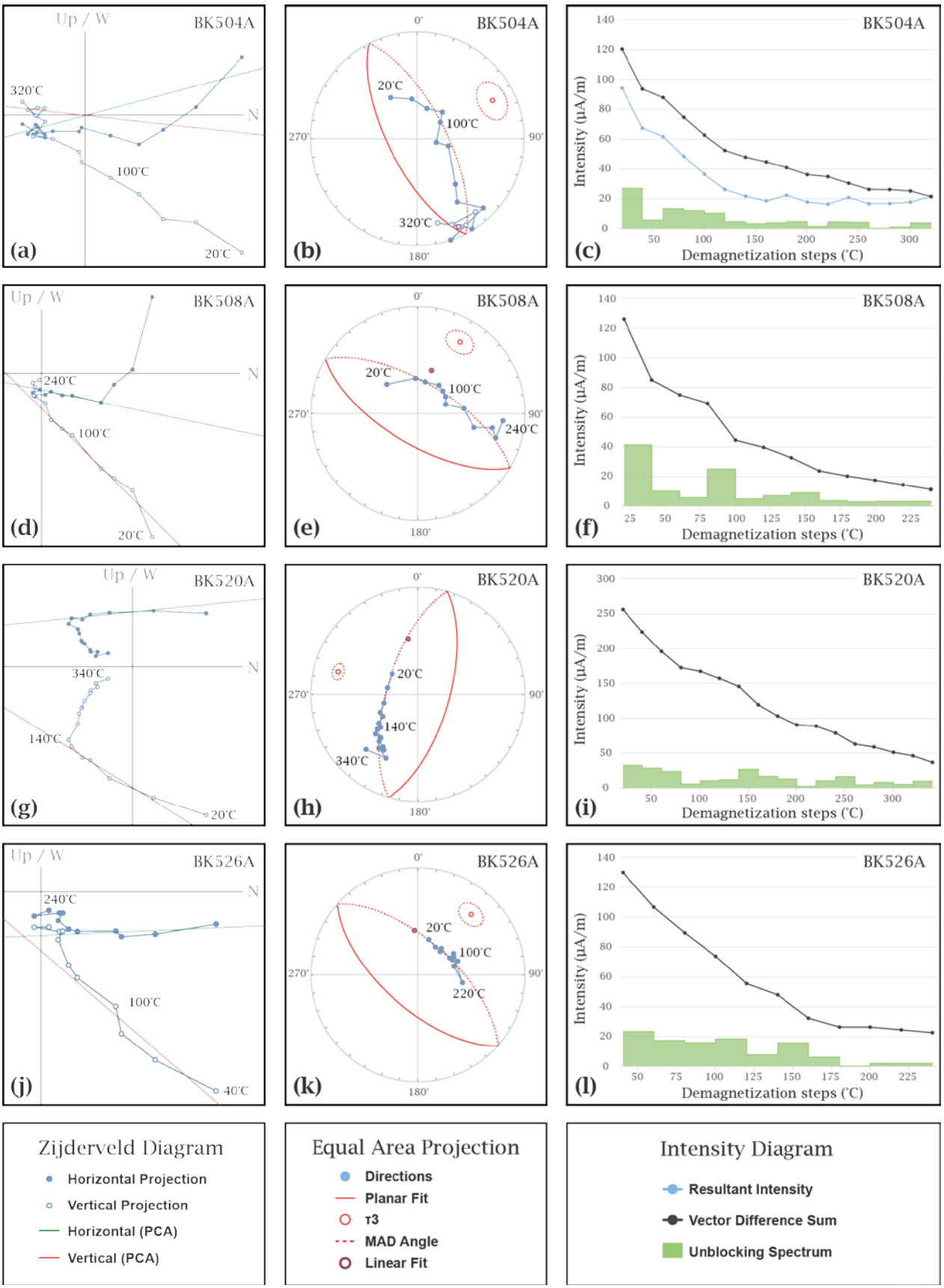
Up / W
BK504A
320°C
100°C
20°C
N
(a)
0°
90°
180°
270°
(b)
(c)
Intensity (μA/m)
Demagnetization steps (°C)
BK508A
240°C
(d)
(e)
(f)
BK520A
340°C
140°C
(g)
(h)
(i)
BK526A
40°C
220°C
(j)
(k)
(l)
Zijderveld Diagram
Horizontal Projection
Vertical Projection
Horizontal (PCA)
Vertical (PCA)
Equal Area Projection
Directions
Planar Fit
τ3
MAD Angle
Linear Fit
Intensity Diagram
Resultant Intensity
Vector Difference Sum
Unblocking Spectrum

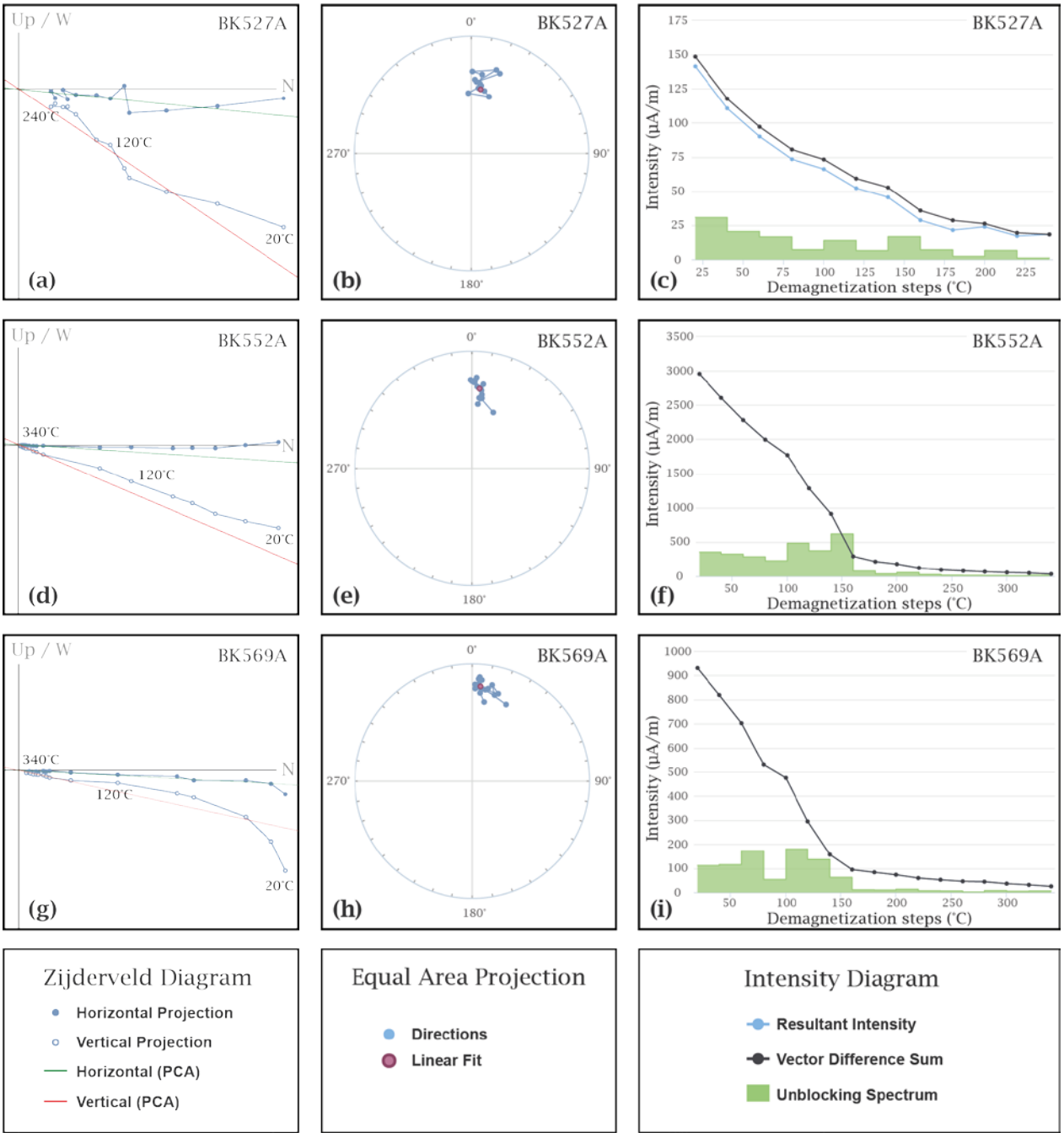

Figure 6. Representative Zijderveld diagrams (TC) with interpretations of high temperature normal directions, equal area projections with clustering of the directions oriented north/down and intensity diagrams showing demagnetization behaviour for specimens BK527A-BK571A from the Pshekha formation.

The specimens of the Belaya Glina formation, which showed unterminated great circle paths and were interpreted to show rotation of the direction of magnetization towards a reversed ChRM, give no direction data that can be used for magnetostratigraphic interpretation. This is why these specimens were assigned expected directions using the interpretation portal of paleomagnetism.org (McFadden and McElhinny, 1988). The direction obtained from specimen BK504A (Figure 5a-c) was used as a set point. A mean direction for these reversed specimens is constructed based on the convergence of these great circles. Consequently a direction for each specimen is constructed based on a best fit to this mean direction and its great circle. Note that this method is not used to show that these specimens have reversed directions, but to construct the most likely lost original directions based on the interpretation that these directions should be reversed. The fitted directions presented in figure 7 are used to construct the inclination and declination graphs in figure 8.

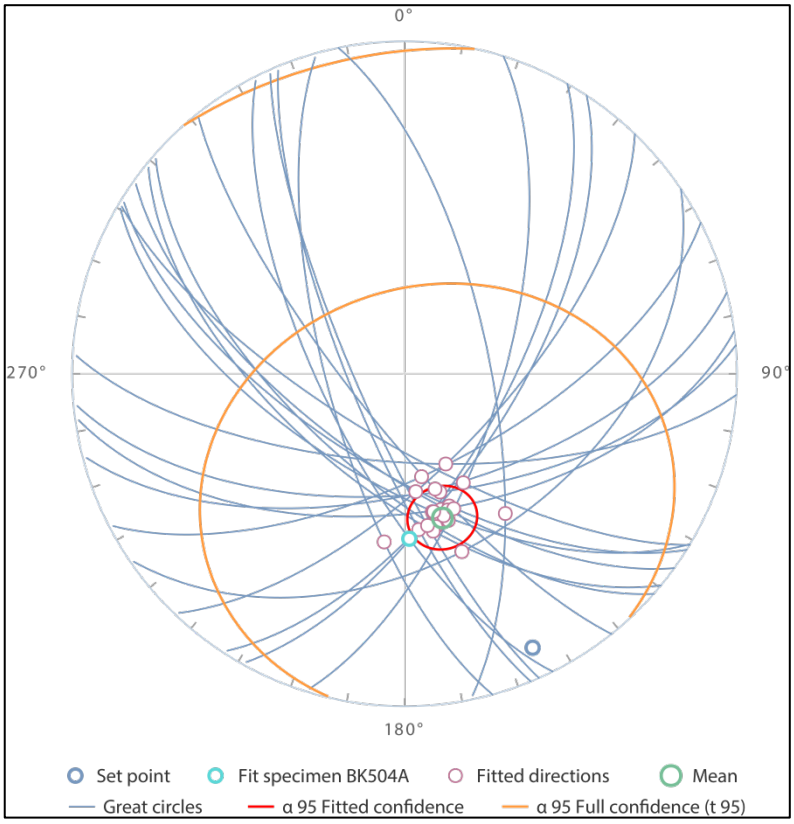

Figure 7. Equal area projection showing all great circle interpretations of the BK500 specimen series and the direction interpreted for specimen BK504A (set point). The mean is the average of all intersections between great circles. Fitted directions are the closest point on each of these great circles to the mean. Constructed with the interpretation portal of paleomagnetism.org (McFadden and McElhinny, 1988).

Figure 8 shows inclination and declination per stratigraphic level and the interpreted polarity pattern. The abnormally low inclination reversed data point is the interpreted direction from specimen BK504A (Figure 5a). This specimen also has a fitted great circle interpretation (Figure 7) which falls more in line with the inclination trend of the reverse polarity specimens. A reversal is observed exactly at the boundary between the Belaya Glina formation and the Pshekha formation. If specimen BK526A (Figure 5j-l, top sample of the Belaya Glina reverse) is interpreted as a normal direction (as suggested above is a possibility) the two samples below could also be interpreted as normal directions since they show similar results. This alternate interpretation would shift the reversal 1 meter down into the Belaya Glina formation. Declination values seem to be stable within this part of the section, but the inclination becomes shallower when going up in the stratigraphy within the Pshekha formation.

Figure 9 shows the expected inclination through time for sections located on the Eurasian plate (GAPWap, Torsvik et al., 2012) in blue. The mean inclination and confidence limits for both the normal polarity and reverse polarity parts of the BK500 series are plotted and do not fall within this expected inclination.

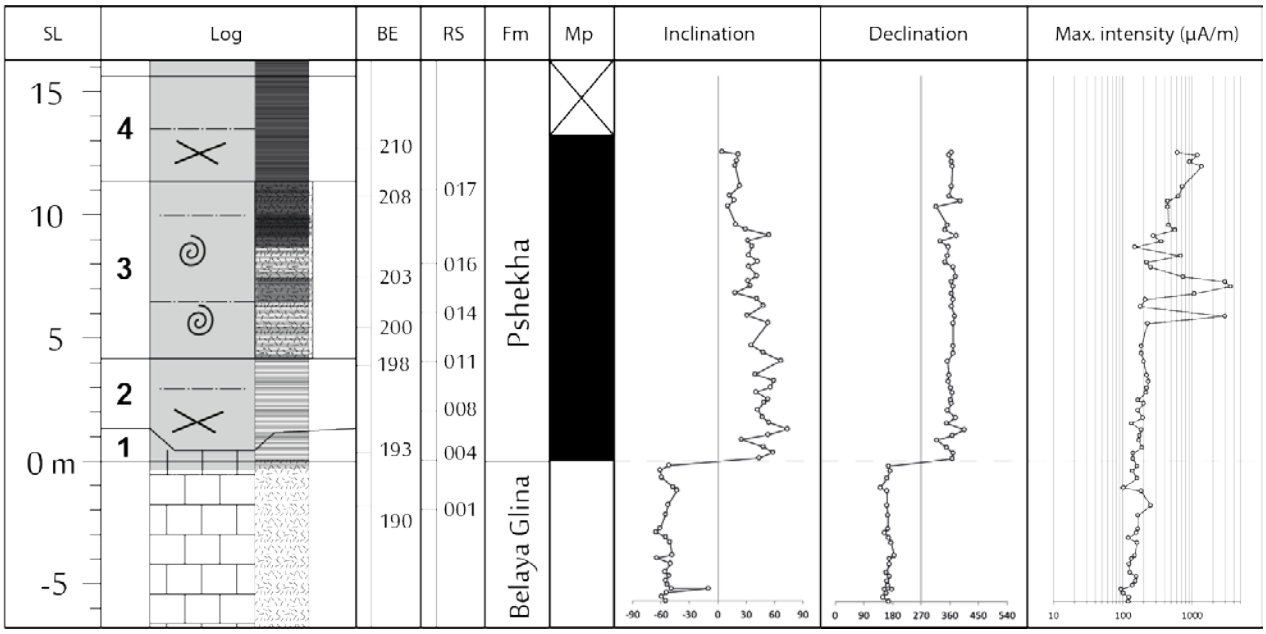

Figure 8. Log for the BK500 series with sample levels for the BE specimen series (Van der Boon, 2017) and the sample levels of the specimens from (Sachsenhofer et al., 2017) in the RS column. SL = stratigraphic level, Mp = interpreted magnetic polarity pattern. The interpreted magnetostratigraphy is based on the declination and inclination graphs for the BK500 series plotted in this figure and consists of a reverse (white) up until the lower boundary of the Pshekha formation and a normal (black) above. The intensity plot shows an increased and more variable initial intensity within the Pshekha formation.

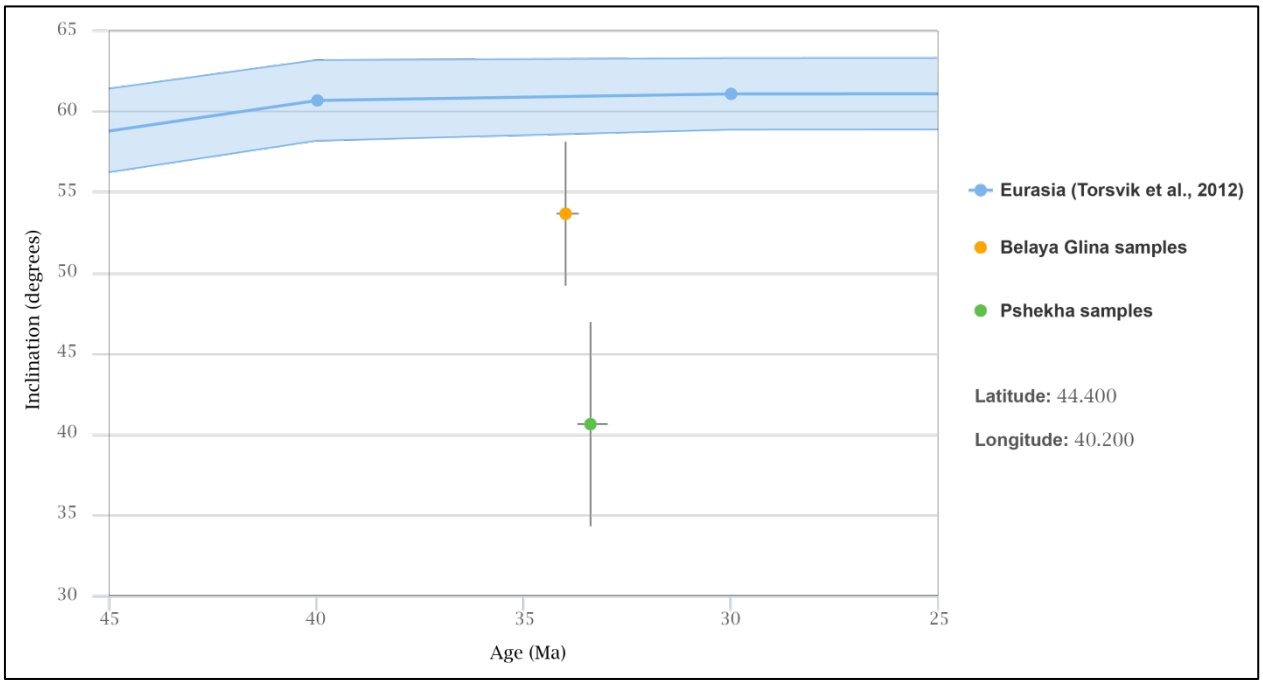

Figure 9. Expected inclination plot with averages for the inclination of specimens from the Belaya Glina formation (converted to normal polarity) and from the Pshekha formation of the BK500 series.

3.2 Dinoflagellate cyst data

Table 1 shows the results of dinoflagellate cyst analysis on several specimens from the Belaya Glina formation (179-189) and the Pshekha formation (193-215).

sample	Dinoflagellate cyst zone	A. diktyoplokum	A. biformoides	M. Pseudorecurvatum	C. funiculatum	E. pectiniforme	A. alcicornu	G. semitecta	L. serrata	R. actinocoronata	W. gochtii
BE215	Rac										X
BE208	Adi	X					X				
BE201	Adi								X		
BE199	Gse							X	X	X	
BE193	?					X					
BE189	Gse (AAl)	X		X		X					
BE184	AAl (Gse)	X			X	X	X				
BE179	AAl		X		X	X					

Table 1. Results of dinoflagellate cyst analysis by A. Grothe. Dinoflagellate cyst zones within brackets are possible but unlikely alternative interpretations of the dinoflagellate compilation.

Dinoflagellate cyst zonations in table 1 are based on (Brinkhuis, 1994; Brinkhuis and Biffi, 1993; Mourik and Brinkhuis, 2005; Pross et al., 2010). A correlation between these zonations and the GPTS is shown in figure 10, showing the Eocene-Oligocene boundary is located in the top of the Aal-zone (Coccioni et al., 2016). *Lentinia serrata* is commonly found within the Adi-zone (Brinkhuis and Biffi, 1993), but the occurrence of *Reticulatosphaera actinocoronata* in sample BE199 indicates this sample belongs to the Gse-zone, since *L. serrata* is also found in the Gse-zone, but *R. actinocoronata* often does not occur in the lower part of the Adi-zone. *Cordosphaeridium funiculatum* has a last occurrence within the bottom of the Gse-zone (Brinkhuis, 1994), but is most common in the AAl-zone (Mourik and Brinkhuis, 2005). The absence of *C. funiculatum* in sample BE189 indicates it probably belongs to the Gse-zone. *Areosphaeridium diktyoplokum* does occur in sample BE184, this species is found in the AAl-zone only at the top, indicating that this sample is close to the AAl-Gse boundary.

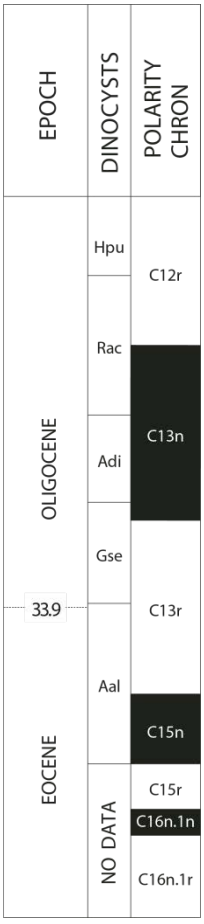

Figure 10. Dinoflagellate cyst zonations and magnetostratigraphy for the Gubbio section (Italy). Figure modified after (Coccioni et al., 2016).

3.3 BK001 and BA series

Figure 11 shows Zijderveld diagrams, equal area projections and intensity diagrams that show the range of demagnetization behaviours found in the rest of the Maikop series. The BA series consists of specimens demagnetized using thermal demagnetization (A specimens) and AF demagnetization (B specimens). Interpretation of the BK001 series was done based on thermally demagnetized specimens and most of the demagnetization behaviours were very similar to those seen in the BK500 series described above (Figures 5 and 6).

Specimens BA288B and BA289A (Figure 11a, b) are from the same stratigraphic level. These specimens show similar and clear demagnetization curves using the different demagnetization methods and are an example of sample levels in the BA series that were interpreted as belonging to a normal chron.

Specimen BK091A (Figure 11c) is an example of a non-interpretable specimen in the BK001 series. This is because the inclination seems to go past the origin possibly towards a reversed direction, however the data points that seem to indicate this have a very low intensity of around 25 μA/m while having a large 95 percent confidence angle of around 20 degrees.

Specimens BA278A, BA278B and BA279B (Figure 11d-f) are from the same stratigraphic level and are an example of a sample level that could not be interpreted. This is because the Zijderveld diagram of the thermally demagnetized specimen BA278A shows a low quality, high temperature normal component while the other two AF demagnetized specimens each show totally different directions.

Specimens BA202A and BK120A (Figure 11g-i) are examples of rare specimens that do not show a normal overprint and give very clear reversed directions. Specimen BK120A also has an exceptionally high initial intensity of 32168 μA/m while still rapidly demagnetizing below 200 °C.

Specimen BK032A (Figure 11j-l) is an example of a specimen showing demagnetization behaviour similar to what the specimens in figure 5 showed; a normal directed NRM, the direction of magnetization moving along a great circle during demagnetization towards a reversed directed ChRM and an initial intensity of 337 μA/m going down to 30 μA/m at 180 °C.

The reversal patterns in figure 12 and 13 are based on the inclination and declination graphs next to it. A large portion of the section is not outcropping in this part of the Maikop, resulting in low sample coverage. The pattern shows a high number of reversals, however, many of these reversals are only defined by one specimen. This is due to the large expected deposition timespan of around 10 My (Palcu et al., 2018; Van der Boon, 2017) for this part of the section and limited amount of samples that were taken for this research. Grey columns in the reversal pattern represent stratigraphic levels that were sampled, but could not be interpreted (e.g. specimen BK091A, figure 11c). Most of the reversed directions were determined using the great circle fitting method described for the BK500 series. This was necessary because of the large influence of a normal overprint in most of the specimens (e.g. specimen BK032A, figure 11j-l).

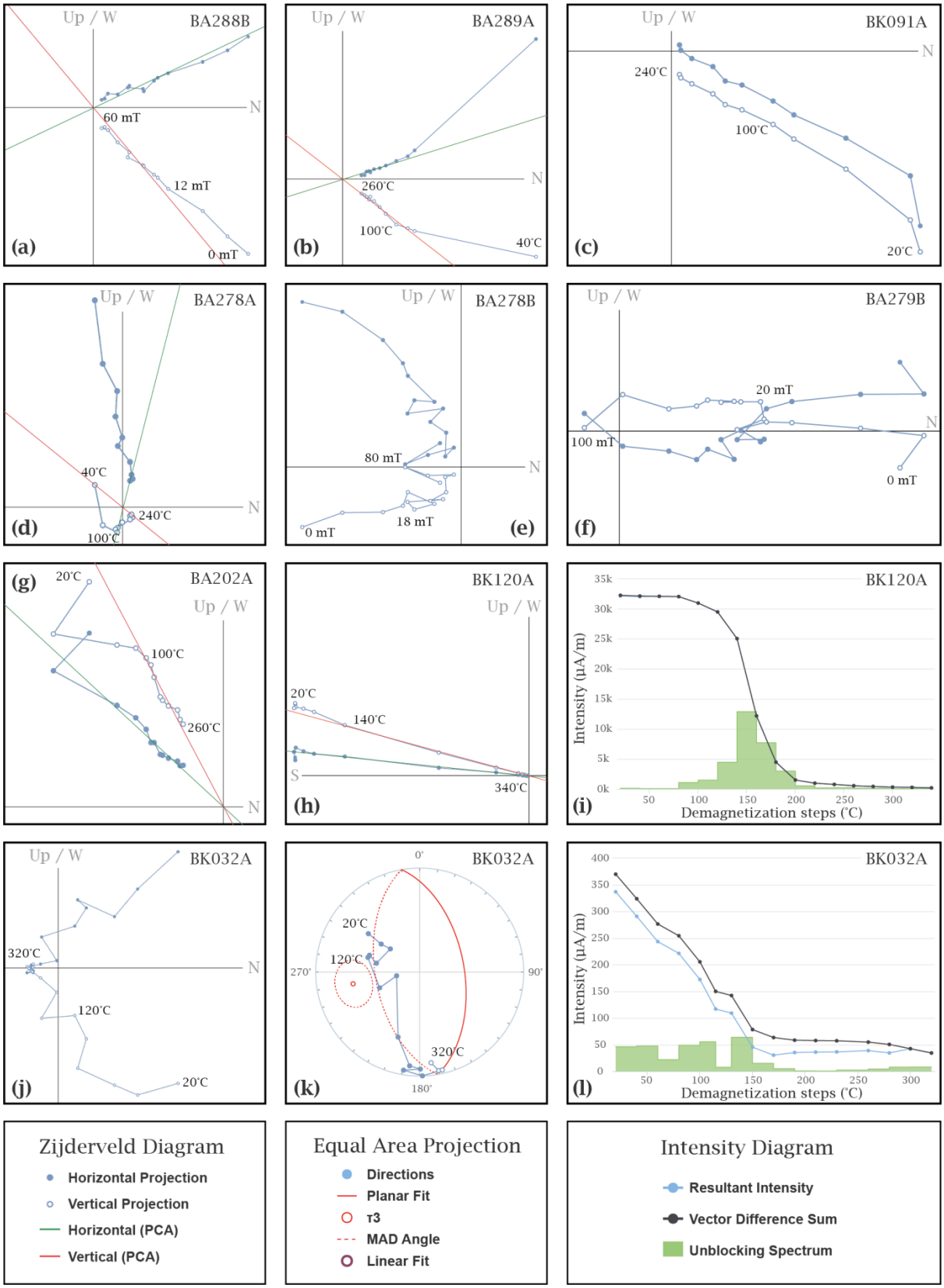

Figure 11. Zijderveld diagrams (TC), equal area projections and intensity diagrams that show the range of demagnetization behaviours found in the BK001 and BA series.

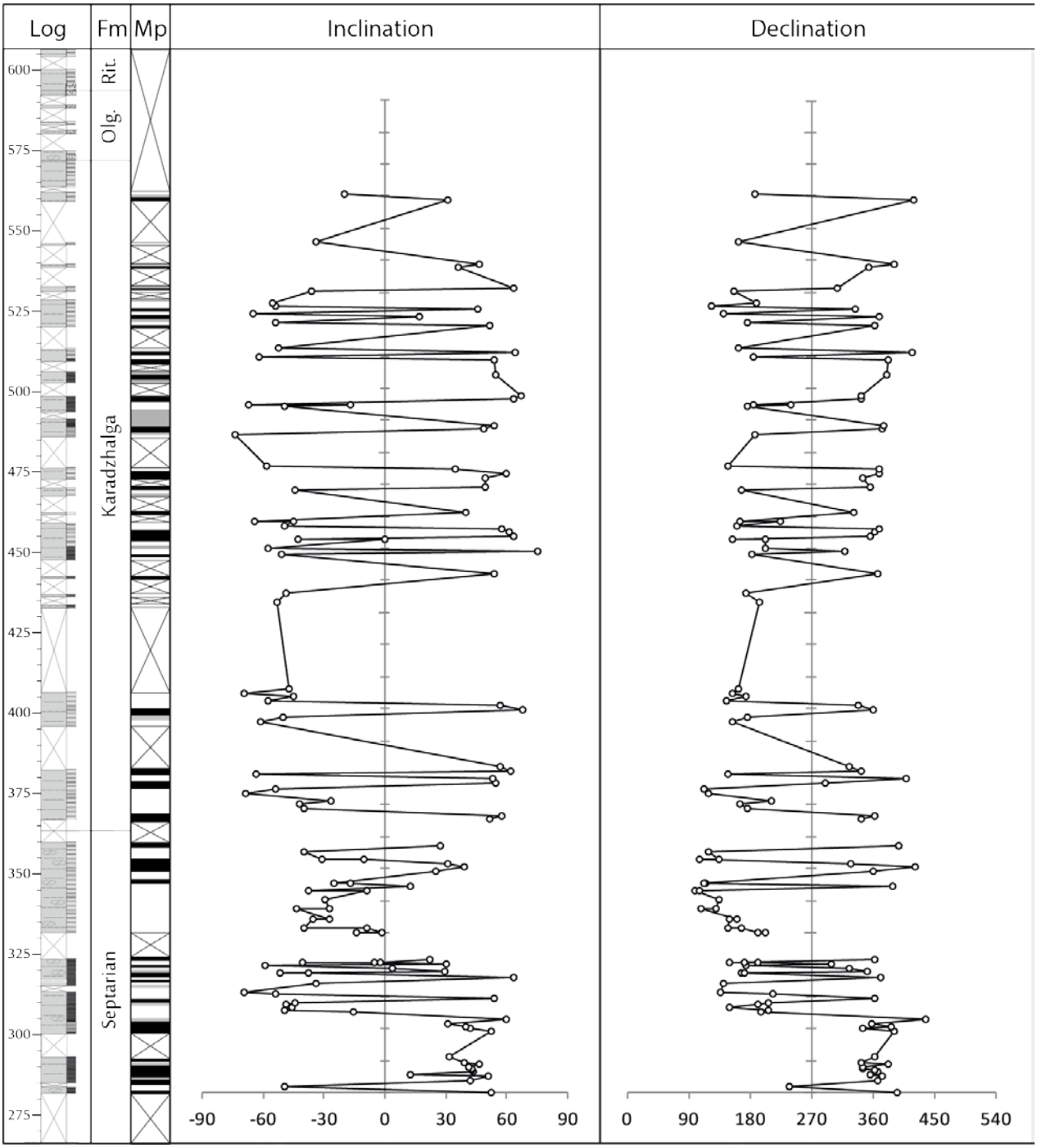

Figure 12. Log for the BK001 series with formations (Fm), inclination and declination graphs and interpreted magnetic polarity pattern (Mp) based on these graphs. Reverse interpreted levels in the magnetostratigraphy are white, normal levels are black, and uninterpreted levels are grey. Olg = Olginskaya, Rit = Ritsa.

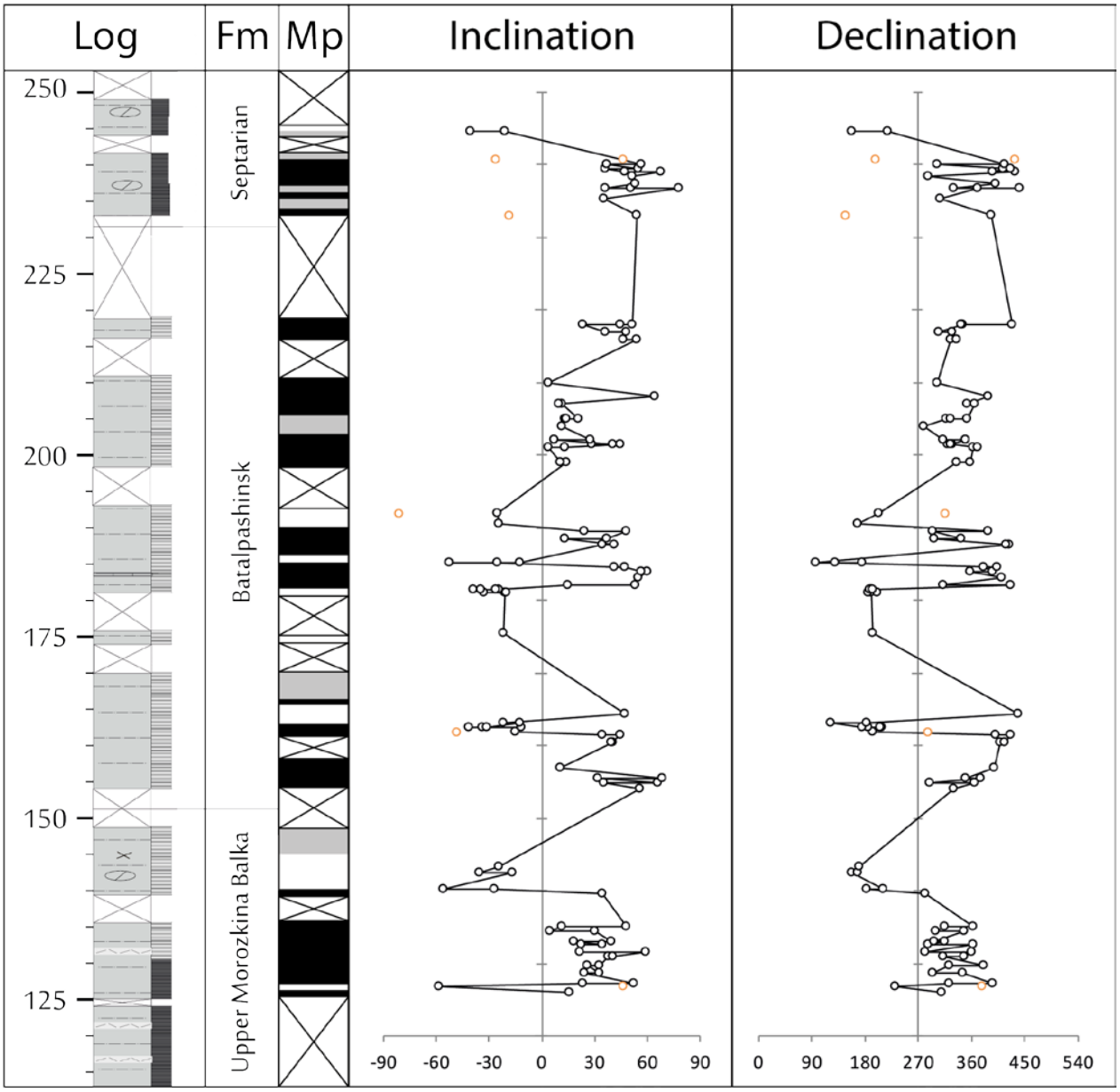

Figure 13. Log for the BA series with, inclination and declination graphs and interpreted magnetic polarity pattern (Mp) based on these graphs. Reversed polarity levels in the magnetostratigraphy are white, normal polarity levels are black and uninterpreted levels are grey. Orange data points indicate specimens with lower quality data.

4. Discussion

4.1 Paleomagnetism

Large parts of the Maikop group are unexposed in this section, or not yet sampled in this study (figure 4). Sample density in most parts of the section is quite low, resulting in interpreted chrons often consisting of only one sample level (figures 12 & 13). Most of the specimens were interpreted to either show a strong normal direction or a reversed ChRM with a significant normal overprint from the Zijderveld plots. However, in most specimens the original signal of sediments deposited during a reverse chron was almost unrecognizable. This, in combination with the low sample density and high amount of reversals, often makes it difficult to show the presence of a reversed chron with certainty. Previous research on the lower Maikop (Van der Boon, 2017) and on the formations overlying the Maikop group (Palcu et al., 2018) give the following two tie points for the correlation between the magnetostratigraphy and the GPTS (figure 14); the normal chron at the bottom of the Maikop is correlated to chron C13n (Van der Boon, 2017) and the magnetostratigraphy above the Maikop (640 to 1200 m in figure 14; after Palcu et al., 2018), correlates with chrons C5AD-C5A (Palcu et al., 2018). This places the upper boundary of the Maikop at approximately 14.86 Ma.

4.2 Biostratigraphy

Calcareous nannoplankton analysis (L.A. Golovina, pers. comm.) indicates that the boundary between nannoplankton zone NP25 and NN1 is located around 350 m, within the Septarian formation (green line in figure 14). This functions as a third tie point for correlation, aged ~23.1 Ma (Vandenberghe et al., 2012). Left of the logs in figure 14 the interpreted biostratigraphic zones (Sachsenhofer et al., 2017 and references therein) for this section are shown.

4.3 Ash layer

(Van der Boon, 2017) dated an ash layer within the Pshekha formation at 33.2 ± 0.34 Ma (2σ) using Ar-Ar dating on biotite grains. This ash layer was correlated to the GPTS using this age, resulting in a location within the GPTS at the top of chron C13n, while the magnetostratigraphic results place this ash layer in the middle of chron C12r. The GPTS (Vandenberghe et al., 2012) ages of chron boundaries, however, are based on astronomical tuning. These ages differ considerably from radio-isotopic ages (e.g. top C13n: astronomic = 33.157 Ma, radio-isotopic = 33.61 Ma). When using the radio-isotopic ages for chron boundaries (Vandenberghe et al., 2012) the ash layer is dated at 19.1% up from the base of chron C12r. If we translate this location in chron C12r to the astronomical time frame the ash layer has an approximate age of 32.75 Ma. The correlation between this new age for the ash layer and its location in the section is shown in figures 14 and 15 with a blue line and is a better fit with the magnetostratigraphy. Astronomic ages are used for the correlation (Figures 14 & 15), since radio-isotopic ages in this part of the GPTS are based on Ar-Ar dating of biotite grains (Vandenberghe et al., 2012). This method has been proven to give anomalously old and less precise ages then when sanadine is used for Ar-Ar dating (Hora et al., 2010).

4.4 Magnetostratigraphy interpretation

Figure 14 shows two possible interpretations based on the combined magnetostratigraphy. The three tie points are used as a starting point for both interpretations. Both interpretations are the same within the Neogene sediments between the tie points at 350 and 640 meters. This part of the section is mostly unexposed, has the lowest sampling rate and the highest frequency of reversals, making exact interpretation difficult. This means that this correlation is one of many possibilities, but based on the available data the most likely one. The correlation of this part of the section to the GPTS was constructed under the assumption that the sedimentation rate was approximately constant. This assumption was made based on the absence of unconformities in outcrops and an approximately constant grainsize in this part of the section (Akhmetiev et al., 1995). The geomagnetic polarity

between the bottom of chron C6B and the top of chron C5B has been tied to observed reversals based on a best fit with this constant sedimentation rate. The correlation of the bottom 350 m in interpretation 1 (Figure 14) is based on the interpretation by (Van der Boon, 2017) in combination with data from (Bogachkin, 2004) indicating a normal polarity for the Polbian sediments, which is interpreted as chron C12n (Zastrozhnov et al., n.d.; pers. comm.). The correlation of these lower 350 m in interpretation 2 (Figure 14) is based on the best fit to a constant sedimentation rate throughout the Maikop group. The fit of C12r in interpretation 2 results in a relatively low sedimentation rate compared to the above chrons, which could be explained by the two erosional events bounding the Polbian level (Sachsenhofer et al., 2017). The dashed black lines at chron boundaries in figure 14 indicate which reversals in the GPTS are correlated to observed reversals in the magnetostratigraphy for each interpretation.

Within both interpretations the bio-zone boundaries that were observed in the section have been extrapolated from the GPTS following the respective magnetostratigraphic correlations (green lines in figure 14). Both interpretations result in the boundary between dinoflagellate cyst zones D15 and D16 falling within the Septarian formation. This is a consequence of the relatively short period between this boundary and the NP25-NN1 calcareous nannofossil zone boundary, which is used as a tie point in both interpretations. This does however show that bio-zone boundaries in this part of the section have a similar configuration as in the GTS (Vandenberghe et al., 2012). There is however a significant difference in the extrapolated stratigraphic height of the boundary between dinoflagellate cyst zones D14 and D15. According to interpretation 1 the top of zone D14 should be within the Lower Morozkina Balka (LMB) formation, while biostratigraphic data suggests the Upper Morozkina Balka (UMB) formation still contains a dinoflagellate cyst assemblage belonging to zone D14b. This zone boundary is located at the top of the UMB according to interpretation 2, which fits with the biostratigraphic data (Sachsenhofer et al., 2017 and references therein). This positive fit between the biostratigraphic zonation as described by (Sachsenhofer et al., 2017) and the zonation from the GTS (Vandenberghe et al., 2012) according to interpretation 2 indicates this correlation is the more reliable one of the two interpretations presented in figure 14. Keep in mind that this reasoning in based on the absence of asynchrony of bio-events which define bio-zone boundaries between the Paratethys and the open oceans. The scarce amount of biostratigraphic data that can be used for dating makes it difficult to determine if this assumption is correct.

The low percentage of Maikop exposed, low sampling density and significant overprint found in reversed specimens results in large uncertainties in the exact stratigraphic levels of reversals in this section. This means interpretation 2 in figure 14 should be seen as an approximation and that the interpretations shown in figure 14 are not the only possible correlations, but only the most probable based on the current available data. This high level of uncertainty is indicated in figure 14 by the grey colour of the correlation between magnetostratigraphy and GPTS. Due to this low quality of the dataset in the middle and upper part of the Maikop this report will further only focus on the discussion of the BK500 series in combination with biostratigraphic data from the lower Maikop.

Figure 14. (next page) Two correllations of composite magnetostratigraphy and biostratigraphy to the geologic time scale (Vandenberghe et al., 2012) based on 1) previous interpretations from (Van der Boon, 2017) and (Zastrozhnov et al., n.d.), 2) approximately constant sedimentation rates and dinoflagellate cyst zones (Dcz). Dashed black lines indicate correlations between observed reversals and reversals in the GPTS. Dashed green lines indicate extrapolation of bio-zone boundaries following the magnetostratigraphic interpretation. The (dashed) blue line represents the ash layer (and its recalculated age). CN = Calcareous nannofossil zones. Half bars in the magnetostratigraphy represent polarities based on single samples, but this representation is only used in the parts of the section with high sample density (below 100 m and above 640 m). See text for further explanation.

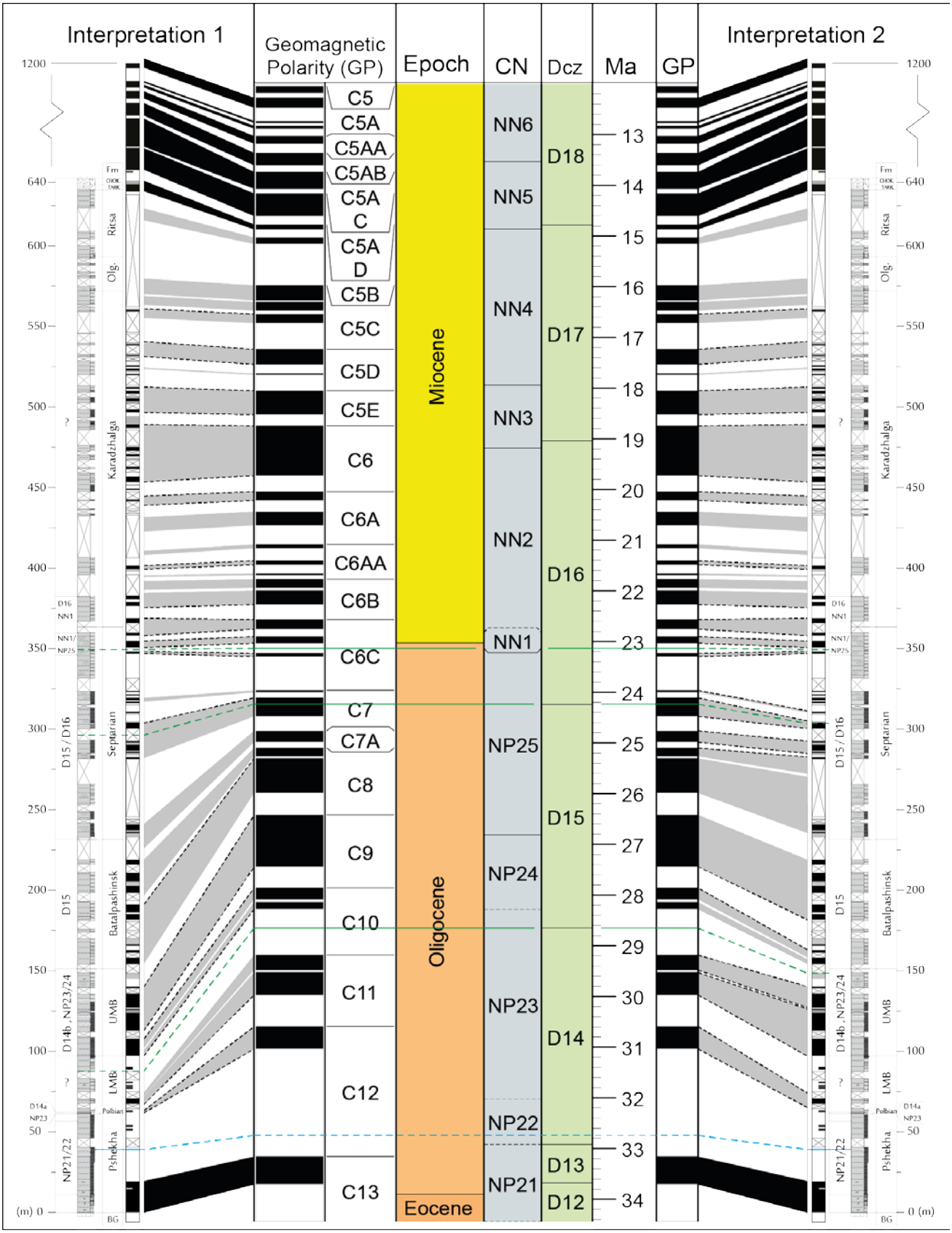
Interpretation 1
Geomagnetic Polarity (GP)
Epoch
CN
Dcz
Ma
GP
Interpretation 2
C5
C5A
C5AA
C5AB
C5AC
C5AD
C5B
C5C
C5D
C5E
C6
C6A
C6AA
C6B
C6C
C7
C7A
C8
C9
C10
C11
C12
C13
Miocene
Oligocene
Eocene
NN6
NN5
NN4
NN3
NN2
NN1
NP25
NP24
NP23
NP22
NP21
D18
D17
D16
D15
D14
D13
D12
13
14
15
16
17
18
19
20
21
22
23
24
25
26
27
28
29
30
31
32
33
34
1200
640
600
550
500
450
400
350
300
250
200
150
100
50
(m) 0
Fm
Ritsa
Olg.
Karadzhalga
Septarian
Batalpashinsk
UMB
LMB
Polbian
Pshekha
BG
D16
NN1
NN1/
NP25
D15 / D16
D15
D14b, NP23/24
D14a
NP23
NP21/22

4.5 BK500 paleomagnetism

The discrepancy between the expected inclination and the mean inclination of this part of the section seen in figure 8 could be explained by inclination shallowing due to compaction. Van der Boon (2017) already showed that using the E-I method (Tauxe et al., 2008) to correct for this shallowing makes enough of a difference within Maikop sediments to adjust for this discrepancy. The dataset analysed in this report however has too few specimens in this part of the section to apply this technique reliably. The shallowing in the inclination going up in the stratigraphy seen in figure 8 could be explained by a too shallow interpretation of these specimens due to a large shallow low temperature component as observed, for example, in BK552A below 160 °C (Figure 6d-f) and in BK569A between 80 and 160 °C (Figure 6g-i). When correlating the magnetostratigraphy in figure 8 to the GPTS (Figure 15), the Belaya Glina-Pshekha boundary falls exactly on the older end of chron C13n, resulting in an age for this boundary of 33.71 Ma (Vandenberghe et al., 2012). Correlation of the upper boundary of chron C13n is based on the polarity pattern from (Van der Boon, 2017; MpB in figure 15), also constructed based on specimens from the Belaya River section, and results in an average sedimentation rate for chron C13n of 3.5 cm/kyr. If a constant sedimentation rate is assumed within the Belaya Glina formation and during chron C13n in figure 15, this correlation with the Geologic Time Scale (GTS; Ogg et al., 2016) results in a stratigraphic height of the Eocene-Oligocene (E/O) boundary 7 meters below the lower boundary of the Maikop Group. However, sedimentation rates are expected to be lower within the Belaya Glina formation (Sachsenhofer et al., 2017; Van der Boon, 2017), 1.3 cm/kyr on average, based on the lower boundary of chron C13n and the identification of the Middle Eocene Climatic Optimum (MECO; ~40.0 Ma) within the underlying Kuma formation (Van der Boon, 2017 and references therein). This would result in a smaller stratigraphic distance between the lower boundary of the Maikop group and the E/O boundary. An exact distance is difficult to determine since this sedimentation rate is an average for approximately 80 meters of section.

4.6 BK500 biostratigraphy

An Oligocene age of the Maikop group lower boundary is not in agreement with (Sachsenhofer et al., 2017), which speculates on the onset of Maikop sedimentation during the late Eocene. However, the placement of the E/O boundary within the Pshekha formation in (Sachsenhofer et al., 2017) is based on the presence of calcareous nannoplankton from zone NP20 (Akhmetiev et al., 1995) in the base of this formation. The age of the upper boundary of zone NP20 is still uncertain (Vandenberghe et al., 2012), which means an Oligocene age for the lower boundary of the Pshekha formation is not excluded by this nannoplankton zone interpretation. According to (Akhmetiev et al., 1995) dinocysts from zone D13 first occur in the Pshekha formation, while the Belaya Glina formation still shows a zone D12 dinocyst compilation. The location of this bio-zone boundary in the section corresponds with the age of this boundary in the GTS in the magnetostratigraphic correlation in figure 15. The dinoflagellate cyst results (table 1) in figure 15 also correspond quite well with the dinoflagellate cyst zones as defined by (Coccioni et al., 2016). Further dinoflagellate cyst studies on the high detail sample set from this study could highly increase the reliability of these zone boundaries. Results from a study by (Gavrilov et al., 2017) on the Chirkei section (Sulak River basin, Northeastern Caucasus) also placed the lower boundary of the Maikop group (the base of the Khadum formation in that study) within the Oligocene, based on zone CNO1 nannoplankton (Agnini et al., 2014; Ogg et al., 2016) found within the Belaya Glina formation. Figure 15 shows the ages of all these biozone boundaries according to the Geologic Time Scale (Ogg et al., 2016) and how they correspond positively to the correlation of the magnetostratigraphy of this research with the GPTS.

4.7 Oi-1 sea level drop

Houben et al. (2012) show that the base of chron C13n coincides with a major sea level drop, the Oi-1 event, of 50-60 meters. This event is seen in oxygen isotope curves as a sharp increase in $\delta^{18}O$ (Figure 15; Cramer et al., 2009; Vandenberghe et al., 2012). It was already hypothesised that the Oi-1 sea level drop caused restriction of the Paratethys from the global oceans (Van der Boon, 2017), the correlation of the start of deposition of oxygen deprived Maikop sediments with the timing of this sea level drop (Figure 15) further cements this hypothesis. Sachsenhofer et al. (2017) describe a major sea level drop at the bottom of the Pshekha formation (Popov et al., 2010), but do not relate this to the Oi-1 event.

4.8 Reliability

The difference in demagnetization behaviour between the Belaya Glina formation and the Pshekha formation that is interpreted as a polarity change in this study might also be ascribed to the difference of sediment composition between these two formations. This, in combination with the low initial intensities and significant normal overprints in the Belaya Glina specimens, creates some uncertainty about the reliability of their interpreted ChRM. However, the locations of bio-zone boundaries in the section when compared to the GPTS suggest the interpretation of the specimens having reverse polarity is correct. The occurrence of a major sea level drop at the base of the Maikop group (Popov et al., 2010) coinciding with the timing of the Oi-1 event at the base of chron C13n in this interpretation, indicating this is the same event, also correlates positively with the reversed polarity interpretation of the Belaya Glina specimens. Even if the C13r-C13n reversal is shifted down 1 meter based on the alternate polarity interpretation of the top three samples of the Belaya Glina formation, the change to deposition of oxygen deprived sediments still occurred during the Oi-1 event. The scenario shown in figure 15 results in Maikop deposition starting at the start of Oi-1, this alternate interpretation would result in Maikop deposition starting at the end of Oi-1.

4.9 Future research

The BK500 series shows that if sample density is high enough it is possible to discern patterns in the demagnetization behaviour of specimens from the Maikop type section that make it possible to infer which specimens with significant normal overprints originally had a reversed signal. Applying such an increased sample density over the rest of the Maikop group in future studies might give paleomagnetic results which make construction of a reliable magnetostratigraphy possible.

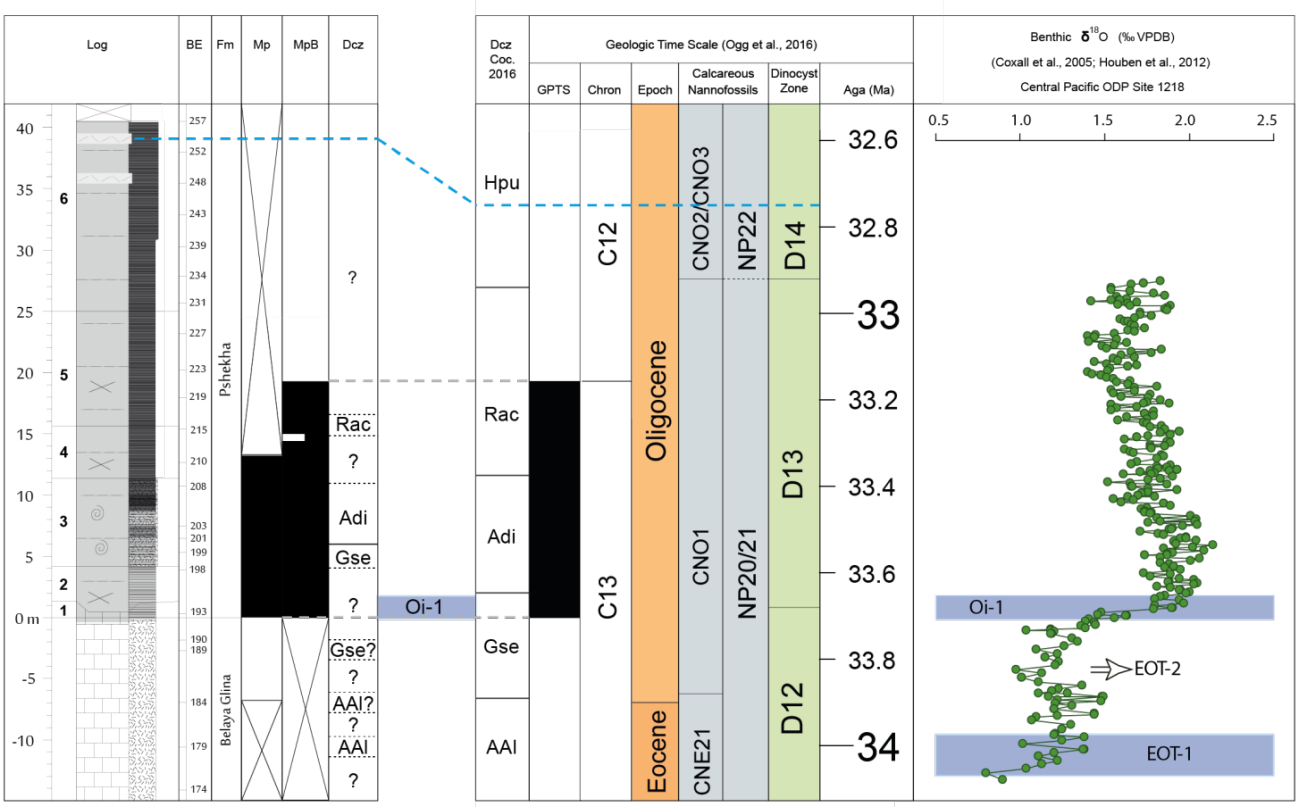

Figure 15. Correlation between the Geologic Time Scale including analysed biostratigrapic boundaries (Ogg et al., 2016) and the log and interpreted magnetic polarity pattern for the BK500 series (Mp). Also included are sample levels for the BE series and their interpretation (MpB; Van der Boon, 2017). The benthic $\delta^{18}O$ curve (Coxall et al., 2005; Houben et al., 2012) shows a rapid positive shift at the base of chron C13n known as the Oi-1 event. This shift in $\delta^{18}O$ is the result of a eustatic sea level drop of 50-60 m (Houben et al., 2012). Dcz = Dinoflagellate cyst zonation results, Dcz Coc. 2016 = Dinoflagellate cyst zones as defined in (Coccioni et al., 2016). Grey dashed lines represent correlations based on magnetostratigraphy. The blue dashed line represents the ash layer with an adjusted age of ~32.75 Ma.

5. Conclusion

The aim of this thesis was to create a magnetostratigraphy for the Maikop type section at the Belaya River and to correlate this magnetostratigraphy to the geologic time scale (GTS). Large gaps in the dataset, low sampling frequency and significant normal overprints made interpretation of directions and correlation to the geologic time scale difficult. By combining the paleomagnetic results with biostratigraphic data and results from other paleomagnetic studies it was, however, possible to construct a most likely correlation between the section and the GTS. This correlation contains large uncertainties, but can be used as a basis for future research into further constraining ages of the Maikop group sediments. A high detail sample set of the base of the Maikop group resulted in a reliable age for the Belaya Glina-Pshekha boundary. This boundary is positioned on the older end of chron C13n, resulting in an age of 33.71 Ma, thus placing the Eocene-Oligocene boundary within the Belaya Glina formation. This means the onset of Maikop sedimentation in a low oxygen environment coincides with a large eustatic sea-level drop, Oi-1 (Figure 15). While large normal overprints affected the specimens from the Belaya Glina formation, the high frequency sampling in this part of the section made it possible to detect a trend in demagnetization behaviour which indicated a reversed ChRM. The recognition of this trend, in combination with information from multiple biostratigraphic data sets, made it possible to accurately determine the location of the base of chron C13n.

Acknowledgements

I would like to thank Annique van der Boon, Niels van Helmond, Robin van der Ploeg, Steven Vincent, Sarah Davies, Michael Morton, Larissa Golovina and Sergey Popov for a fantastic and well organized fieldwork and for helping and guiding in any way they could during the remainder of my thesis project. I would also like to thank Evgeni and Irina for the amazing care, service and meals during this fieldwork. I would also like to thank Wout Krijgsman, Mark Dekkers and Cor Langereis for their guidance and feedback and all the other staff, researchers and students at Fort Hoofddijk for being there to bounce off ideas and exchange feedback. And a final thanks for Arjen Grothe for his work on dinoflagellate cysts.

References

Agnini, C., Fornaciari, E., Raffi, I., Catanzariti, R., Pälike, H., Backman, J., Rio, D., 2014. Biozonation and biochronology of Paleogene calcareous nannofossils from low and middle latitudes. Newsletters Stratigr. 47, 131–181. https://doi.org/10.1127/0078-0421/2014/0042

Akhmetiev, M.A., Popov, S.V., Krhovsky, J., Goncharova, I.A., Zaporozhets, N.I., Sychevskaya, E.K., Radionova, E.P., 1995. Palaeontology and Stratigraphy of the Eocene–Miocene Sections of the Western Pre-Caucasia: Excursion Guidebook.

Allen, M.B., Armstrong, H.A., 2008. Arabia–Eurasia collision and the forcing of mid-Cenozoic global cooling. Palaeogeogr. Palaeoclimatol. Palaeoecol. 265, 52–58. https://doi.org/10.1016/J.PALAEO.2008.04.021

Bogachkin, A.B., 2004. Paleomagnetic stratigraphy and petromagnetism of the paleogenic sediments of Caucasus and Northern Pre-Caspian. N. G. Chernyshevsky Saratov State Univesrity.

Brinkhuis, H., 1994. Late Eocene to Early Oligocene dinoflagellate cysts from the Priabonian type-area (Northeast Italy): biostratigraphy and paleoenvironmental interpretation. Palaeogeogr. Palaeoclimatol. Palaeoecol. 107, 121–163. https://doi.org/10.1016/0031-0182(94)90168-6

Brinkhuis, H., Biffi, U., 1993. Dinoflagellate cyst stratigraphy of the Eocene/Oligocene transition in central Italy. Mar. Micropaleontol. 22, 131–183. https://doi.org/10.1016/0377-8398(93)90007-K

Brinkhuis, H., Sengers, S., Sluijs, A., Warnaar, J., Williams, G.L., 2003. L Atest C Retaceous – E Arliest O Ligocene and Q Uaternary D Inoflagellate C Ysts , Odp S Ite 1172 , 189.

Coccioni, R., Catanzariti, R., Frontalini, F., Galbrun, B., Jovane, L., Montanari, A., Savian, J.F., Sideri, M., 2016. Integrated magnetostratigraphy, biostratigraphy, and chronostratigraphy of the Paleogene pelagic succession at Gubbio (central Italy). Geol. Soc. Am. Spec. Pap. 524 2524, 139–160. https://doi.org/10.1130/2016.2524(10).

Coxall, H.K., Wilson, P.A., Pälike, H., Lear, C.H., Backman, J., 2005. Rapid stepwise onset of Antarctic glaciation and deeper calcite compensation in the Pacific Ocean. Nature 433, 53–57. https://doi.org/10.1038/nature03135

Cramer, B.S., Toggweiler, J.R., Wright, J.D., Katz, M.E., Miller, K.G., 2009. Ocean overturning since the late cretaceous: Inferences from a new benthic foraminiferal isotope compilation. Paleoceanography 24, 1–14. https://doi.org/10.1029/2008PA001683

Ershov, A. V., Brunet, M.-F., Korotaev, M. V., Nikishin, A.M., N. Bolotov, S., 1999. Late Cenozoic burial history and dynamics of the Northern Caucasus molasse basin: implications for foreland basin modelling. Tectonophysics 313, 219–241. https://doi.org/10.1016/S0040-1951(99)00197-3

Ershov, A. V., Brunet, M.-F., Nikishin, A.M., Bolotov, S.N., Nazarevich, B.P., Korotaev, M. V., 2003. Northern Caucasus basin: thermal history and synthesis of subsidence models. Sediment. Geol. 156, 95–118. https://doi.org/10.1016/S0037-0738(02)00284-1

Fischer, R.F.S., 1953. Dispersion on a sphere. Proc. R. Soc. London A Math. Phys. Eng. Sci. 217, 295–305. https://doi.org/10.1098/rspa.1953.0064

Gavrilov, Y.O., Shchepetova, E. V., Shcherbinina, E.A., Golovanova, O. V., Nedumov, R.I., Pokrovsky, B.G., 2017. Sedimentary environments and geochemistry of Upper Eocene and Lower Oligocene rocks in the northeastern Caucasus. Lithol. Miner. Resour. 52, 447–466. https://doi.org/10.1134/S0024490217060037

Hora, J.M., Singer, B.S., Jicha, B.R., Beard, B.L., Johnson, C.M., de Silva, S., Salisbury, M., 2010. Volcanic biotite-sanidine40Ar/39Ar age discordances reflect Ar partitioning and pre-eruption closure in biotite. Geology 38, 923–926. https://doi.org/10.1130/G31064.1

Houben, A.J.P., van Mourik, C.A., Montanari, A., Coccioni, R., Brinkhuis, H., 2012. The Eocene–Oligocene transition:

Changes in sea level, temperature or both? Palaeogeogr. Palaeoclimatol. Palaeoecol. 335–336, 75–83. https://doi.org/10.1016/J.PALAEO.2011.04.008
Hudson, S.M., Johnson, C.L., Efendiyeva, M.A., Rowe, H.D., Feyzullayev, A.A., Aliyev, C.S., 2008. Stratigraphy and geochemical characterization of the Oligocene–Miocene Maikop series: Implications for the paleogeography of Eastern Azerbaijan. Tectonophysics 451, 40–55. https://doi.org/10.1016/J.TECTO.2007.11.045
Kirschvink, J.L., 1980. The least-square line and plane and the analysis of paleomagnetic data. Geophys. J. R. Astron. Soc. 62, 699–718. https://doi.org/10.1111/j.1365-246X.1980.tb02601.x
Koymans, M.R., Langereis, C.G., Pastor-Galán, D., van Hinsbergen, D.J.J., 2016. Paleomagnetism.org: An online multi-platform open source environment for paleomagnetic data analysis. Comput. Geosci. 93, 127–137. https://doi.org/10.1016/J.CAGEO.2016.05.007
McFadden, P.L., McElhinny, M.W., 1988. The combined analysis of remagnetization circles and direct observations in palaeomagnetism. Earth Planet. Sci. Lett. 87, 161–172. https://doi.org/10.1016/0012-821X(88)90072-6
Mourik, C. Van, Brinkhuis, H., 2005. The Massignano Eocene-Oligocene golden spike section revisited. Stratigraphy 2, 13–29.
Mullender, T.A.T., Frederichs, T., Hilgenfeldt, C., de Groot, L. V., Fabian, K., Dekkers, M.J., 2016. Automated paleomagnetic and rock magnetic data acquisition with an in-line horizontal “2G” system. Geochemistry, Geophys. Geosystems 17, 3546–3559. https://doi.org/10.1002/2016GC006436
Ogg, J.G., Ogg, G.M., Gradstein, F.M., Ogg, J.G., Ogg, G.M., Gradstein, F.M., 2016. Paleogene, in: A Concise Geologic Time Scale. Elsevier, pp. 187–201. https://doi.org/10.1016/B978-0-444-59467-9.00014-5
Palcu, D.V., Popov, S.V., Golovina, L.A., Kuiper, K.F., Liu, S., Krijgsman, W., 2018. The shutdown of an anoxic giant: magnetostratigraphic dating of the end of the Maikop Sea. Palaeogeogr. Palaeoclimatol. Palaeoecol. In press.
Popov, S.V., Rögl, F., Rozanov, A.Y., Steininger, F.F., Shcherba, I.G., Kovac, M., 2004. Lithological-Paleogeographic maps of Paratethys 10 maps Late Eocene to Pliocene. Schweizerbart Science Publishers, Stuttgart, Germany.
Popov, S. V., Antipov, M.P., Zastrozhnov, A.S., Kurina, E.E., Pinchuk, T.N., 2010. Sea-level fluctuations on the northern shelf of the Eastern Paratethys in the Oligocene-Neogene. Stratigr. Geol. Correl. 18, 200–224. https://doi.org/10.1134/S0869593810020073
Pross, J., Houben, A.J.P., van Simaeys, S., Williams, G.L., Kotthoff, U., Coccioni, R., Wilpshaar, M., Brinkhuis, H., 2010. Umbria–Marche revisited: A refined magnetostratigraphic calibration of dinoflagellate cyst events for the Oligocene of the Western Tethys. Rev. Palaeobot. Palynol. 158, 213–235. https://doi.org/10.1016/J.REVPALBO.2009.09.002
Sachsenhofer, R.F., Popov, S. V., Akhmetiev, M.A., Bechtel, A., Gratzer, R., Groß, D., Horsfield, B., Rachetti, A., Rupprecht, B., Schaffar, W.B.H., Zaporozhets, N.I., 2017. The type section of the Maikop Group (Oligocene-lower Miocene) at the Belaya River (North Caucasus): Depositional environment and hydrocarbon potential. Am. Assoc. Pet. Geol. Bull. 101, 289–319. https://doi.org/10.1306/08051616027
Sachsenhofer, R.F., Schulz, H.-M., 2006. Architecture of Lower Oligocene source rocks in the Alpine Foreland Basin: a model for syn- and post-depositional source-rock features in the Paratethyan realm. Pet. Geosci. 12, 363–377. https://doi.org/10.1144/1354-079306-712
Schulz, H.-M., Bechtel, A., Sachsenhofer, R.F., 2005. The birth of the Paratethys during the Early Oligocene: From Tethys to an ancient Black Sea analogue? Glob. Planet. Change 49, 163–176. https://doi.org/10.1016/J.GLOPLACHA.2005.07.001
Tauxe, L., Kodama, K.P., Kent, D.V., 2008. Testing corrections for paleomagnetic inclination error in sedimentary rocks: A comparative approach. Phys. Earth Planet. Inter. 169, 152–165. https://doi.org/10.1016/J.PEPI.2008.05.006
Torsvik, T.H., Van der Voo, R., Preeden, U., Mac Niocaill, C., Steinberger, B., Doubrovine, P. V., van Hinsbergen, D.J.J., Domeier, M., Gaina, C., Tohver, E., Meert, J.G., McCausland, P.J.A., Cocks, L.R.M., 2012. Phanerozoic polar wander, palaeogeography and dynamics. Earth-Science Rev. 114, 325–368. https://doi.org/10.1016/J.EARSCIREV.2012.06.007
Van der Boon, A., 2017. From Peri-Tethys to Paratethys : Basin restriction and anoxia in central Eurasia linked to volcanic belts in Iran. Utrecht studies in earth sciences No. 142.
Van Hinsbergen, D.J.J., De Groot, L. V., Van Schaik, S.J., Spakman, W., Bijl, P.K., Sluijs, A., Langereis, C.G., Brinkhuis, H., 2015. A paleolatitude calculator for paleoclimate studies. PLoS One 10, 1–21. https://doi.org/10.1371/journal.pone.0126946
Vandenberghe, N., Hilgen, F.J., Speijer, R.P., Ogg, J.G., Gradstein, F.M., Hammer, O., Hollis, C.J., Hooker, J.J., 2012.

The Paleogene Period, in: The Geologic Time Scale. Elsevier, pp. 855–921. https://doi.org/10.1016/B978-0-444-59425-9.00028-7
Varentsov, I.M., Muzyliov, N.G., Nikolaev, V.G., Stupin, S.I., 2003. The origin of black shale-hosted Mn deposits in Paratethyan basins: Constraints from geological events at the Eocene/Oligocene boundary. Russ. J. Earth Sci. 5, 255–272. https://doi.org/10.2205/2003ES000129
Zastrozhnov, A.S., Popov, S.V., Benyamovsky, V.N., Musatov, V.A., Akhmet'ev, M.A., Zaporozhets, N.I., Bogachkin, A.B., Stolyarov, A.S., Ivleva, E.I., n.d. Oligocene key section of northern ergeny. Stratigr. Geol. Correl. in press.
Zijderveld, J.D.A., 1967. A. C. Demagnetization of Rocks: Analysis of Results. Methods Paleomagn. 254–286.